Molecular Vision 2024; 30:17-35 <http://www.molvis.org/molvis/v30/17>
Received 18 September 2023 | Accepted 7 February 2024 | Published 10 February 2024

Central subfield thickness of diabetic macular edema: Correlation with the aqueous humor proteome

Lasse Jørgensen Cehofski,[1,2] Kentaro Kojima,[3] Natsuki Kusada,[3] Mathilde Schlippe Hansen,[1] Danson Vasanthan Muttuvelu,[4,5] Noëlle Bakker,[6] Ingeborg Klaassen,[6] Jakob Grauslund,[1,2] Henrik Vorum,[7,8] Bent Honoré[8,9]

[1]Department of Ophthalmology, Odense University Hospital, Odense, Denmark; [2]Department of Clinical Research, University of Southern Denmark, Odense, Denmark; [3]Department of Ophthalmology, Kyoto Prefectural University of Medicine, Kyoto, Japan; [4]Department of Ophthalmology, Mitoje Aps, Skive, Denmark; [5]University of Copenhagen, Faculty of Health Sciences, Copenhagen, Denmark; [6]Ocular Angiogenesis Group, Department of Ophthalmology, Amsterdam UMC location University of Amsterdam, Amsterdam, The Netherlands; [7]Department of Ophthalmology, Aalborg University Hospital, Aalborg, Denmark; [8]Department of Clinical Medicine, Aalborg University, Aalborg, Denmark; [9]Department of Biomedicine, Aarhus University, Aarhus, Denmark

Purpose: Diabetic macular edema (DME) is a sight-threatening complication of diabetes. Consequently, studying the proteome of DME may provide novel insights into underlying molecular mechanisms.

Methods: In this study, aqueous humor samples from eyes with treatment-naïve clinically significant DME (n = 13) and age-matched controls (n = 11) were compared with label-free liquid chromatography–tandem mass spectrometry. Additional aqueous humor samples from eyes with treatment-naïve DME (n = 15) and controls (n = 8) were obtained for validation by enzyme-linked immunosorbent assay (ELISA). Best-corrected visual acuity (BCVA) was evaluated, and the severity of DME was measured as central subfield thickness (CST) employing optical coherence tomography. Control samples were obtained before cataract surgery. Significantly changed proteins were identified using a permutation-based calculation, with a false discovery rate of 0.05. A human donor eye with DME and a control eye were used for immunofluorescence.

Results: A total of 101 proteins were differentially expressed in the DME. Regulated proteins were involved in complement activation, glycolysis, extracellular matrix interaction, and cholesterol metabolism. The highest-fold change was observed for the fibrinogen alpha chain (fold change = 17.8). Complement components C2, C5, and C8, fibronectin, and hepatocyte growth factor-like protein were increased in DME and correlated with best-corrected visual acuity (BCVA). Ceruloplasmin and complement component C8 correlated with central subfield thickness (CST). Hemopexin, plasma kallikrein, monocyte differentiation antigen CD14 (CD14), and lipopolysaccharide-binding protein (LBP) were upregulated in the DME. LBP was correlated with vascular endothelial growth factor. The increased level of LBP in DME was confirmed using ELISA. The proteins involved in desmosomal integrity, including desmocollin-1 and desmoglein-1, were downregulated in DME and correlated negatively with CST. Immunofluorescence confirmed the extravasation of fibrinogen at the retinal level in the DME.

Conclusion: Elevated levels of pro-inflammatory proteins, including the complement components LBP and CD14, were observed in DME. DME was associated with the loss of basal membrane proteins, compromised desmosomal integrity, and perturbation of glycolysis.

Clinically significant diabetic macular edema (DME) is the leading cause of visual impairment in diabetic patients and may occur in any state of diabetic retinopathy [1–3]. As the prevalence of diabetes is estimated to reach almost 600 million people by 2030, the number of DME cases is expected to grow throughout the upcoming decades [4,5]. DME results from the disruption of the blood–retinal barrier with increased vascular permeability and leakage of fluid into the macular area [6]. Increased vascular permeability is mediated by vascular endothelial growth factor (VEGF), and an inflammatory response is driven by proinflammatory cytokines [6]. DME is effectively treated by neutralizing VEGF with intravitreal anti-VEGF agents, which are regarded as first-line therapy [7], with dexamethasone intravitreal implants often used as second-line therapy in the management of DME [5]. Despite therapeutic advances, DME remains a significant burden. Patients with diabetes often have multiple pluridisciplinary appointments with the healthcare system [8]. DME often recurs, and re-treatments with frequent follow-up visits are often necessary [7].

Knowledge about protein-driven processes that contribute to visual loss and the macular accumulation of

Correspondence to: Lasse Jørgensen Cehofski, Department of Ophthalmology, Odense University Hospital Sdr. Boulevard 29, 5000 Odense, Denmark. Phone +45 53558878 email: Lassecehofski@hotmail.com

fluid may lead to advances in the management of DME. As observed in our recent review [9], most proteome studies of DME date to a decade ago. In recent years, major advances have been made in proteomic techniques, including sample preparation, liquid chromatography, and mass spectrometry. These significant advances are leading to greater depth in proteome analyses with the discovery of novel protein-driven disease mechanisms [10–12]. We have recently demonstrated that the aqueous humor proteome correlates with clinical parameters in branch retinal vein occlusion (BRVO) and central retinal vein occlusion (CRVO) [13,14]. Knowledge about the aqueous humor proteome and its correlation to clinical parameters in DME is very limited [9]. Here, we report on the aqueous humor proteome of DME and its correlations with clinical parameters using advanced proteomic approaches.

METHODS

Samples: This study was conducted in compliance with the Institutional Review Board of Kyoto Prefectural University of Medicine, from which approval for the study was obtained (permission RBMR-C-864–6). The study adhered to the tenets of the Helsinki Declaration. Informed consent to use samples from the biobank was obtained from all patients after an explanation of the nature and possible consequences of the study.

Aqueous humor samples from eyes with treatment-naïve clinically significant DME (n = 13) and age-matched controls (n = 11) were donated from the biobank of Kyoto Prefectural University Hospital, Kyoto, Japan (Table 1). Normal distribution was assessed in STATA 16.0 (StataCorp, College Station, TX) with histograms and the skewness and kurtosis test for normality referred to in STATA 16.0 as the sktest. The Student's t test was used to confirm that there was no statistically significant difference in age between the two groups (Table 1). Fisher's exact test was used for categorical data. All patients in the DME group had clinically significant treatment-naïve DME. In the DME group, the exclusion criteria were iris rubeosis, hyphema, glaucoma (including neovascular glaucoma), vitreous hemorrhage, previous anti-VEGF treatment, central laser, and periocular or intraocular corticosteroid injections. Control samples were obtained before cataract surgery from age-matched patients who had no ocular disease other than cataract. Best-corrected visual acuity (BCVA) was measured as the logarithm of the minimum angle of resolution (logMAR). Optical coherence tomography (OCT) was obtained with Swept Source OCT (DRI-OCT Triton; Topcon, Tokyo, Japan). The severity of DME was measured as central subfield thickness (CST) with the caliber tool of Topcon OCT software (DRI-OCT Triton; Topcon, Tokyo, Japan).

Table 1. Samples for proteomic analysis.

Various	DME	Control	p-value
Number of samples (n)	13*	11	
Patients (n)	11		
Age (years)	61.9±18.7	68.5±11.3	0.32
Sex (M/F)	5/8	5/6	
BCVA (logMAR)	0.48±0.25		
Central subfield thickness (µm)	366.9±176.0		
Mild non-proliferative diabetic retinopathy (n)	1		
Moderate non-proliferative diabetic retinopathy (n)	3		
Severe non-proliferative diabetic retinopathy (n)	3		
Proliferative diabetic retinopathy (n)	6		
HbA1c (%)	8.1±2.0		
Hypertension (n)	10	2	0.012
Hyperlipidemia (n)	6	2	0.21
Oral treatment (n)	11		
Oral treatment and insulin (n)	4		
Insulin, no oral treatment (n)	0		
Creatinin mg/dl	1.71±1.37	0.76±0.15	0.023

*Two patients participated with both eyes.

Additional aqueous humor samples from eyes with treatment-naïve DME (n = 15) and control samples (n = 8) were obtained from the biobank for validation by ELISA (Table 2). Normal distribution was assessed in STATA 16.0 (StataCorp, College Station, TX) with histograms and the skewness and kurtosis test for normality, referred to in STATA 16.0 as the sktest. The Mann–Whitney U test was used to confirm that there was no statistical difference in age between the groups (Table 2). Fisher's exact test was used for categorical data. Samples obtained for validation by ELISA were selected according to the inclusion and exclusion criteria that were applied to samples attained for proteomic analysis by mass spectrometry.

Sample preparation for mass spectrometry: The samples were stored at −80 °C until sample preparation was initiated. The protein concentration was measured using an infrared spectrometer (Direct Detect, Darmstadt, Germany). Sample

Table 2. Samples for validation by ELISA.

Various	DME ELISA	Control	P-value
Number of samples	15	8	
Patients	15	7	
Age (years)	65.2±15.1	71.0±9.3	0.32
Sex (M/F)	9/6	4/4	
BCVA (logMAR)	0.44±0.28		
Central subfield thickness (µm)	384.5±161.9		
Mild non-proliferative diabetic retinopathy (n)	2		
Moderate non-proliferative diabetic retinopathy (n)	4		
Severe non-proliferative diabetic retinopathy (n)	4		
Proliferative diabetic retinopathy (n)	5		
HbA1c (%)	7.9±1.82		
Hypertension (n)	10	3	0.22
Hyperlipidemia (n)	5	0	0.12
Oral treatment (n)	14		
Oral treatment and insulin (n)	4		
Insulin, no oral treatment (n)	0		
Creatinin (mg/dl)	1.31±0.95	0.82±0.12	0.11

preparation was performed according to the S-Trap micro-spin column digestion protocol (ProtiFi, Huntington, NY, USA). The volume of each sample was measured, and an equal volume of 2 x SDS lysis buffer (10% SDS, 100 mM triethylammonium bicarbonate [TEAB], pH 8.5) was added. Reduction was performed by adding tris(2-carboxyethyl) phosphine hydrochloride (TCEP) to the protein solution in SDS for a final concentration of 10 mM, followed by heating for 10 min at 95 °C. The protein solution was cooled to room temperature, followed by alkylation by adding iodoacetamide. A 12% aqueous phosphoric acid solution at 1:10 was added to reach a final concentration of 1.2% phosphoric acid. S-Trap binding buffer (90% methanol, 100 mM TEAB) was added. The samples were transferred to microcolumns and centrifuged at 4,000 ×*g* until the buffer passed through the S-Trap column. S-Trap binding buffer was added, and centrifugation at 4,000*g* was performed three times. The S-Trap microcolumn was moved to a new 1.7 ml sample tube, and 20 µl of digestion buffer was added, followed by incubation overnight at 37 °C. Elution was first performed with 40 µl of 50 mM TEAB and then with 0.2% formic acid, followed by centrifugation at 4,000 ×*g*. The recovery of hydrophobic peptides was performed with an elution of 35 µl of 50% acetonitrile containing 0.2% formic acid. Elutions were pooled, and the peptide concentration was measured using a fluorescence-based technique with tryptophan as a standard, with an excitation at 295 nm and emission at 350 nm, as previously described [15]. The samples were dried in a vacuum centrifuge and stored at −80 °C until further use.

Quantitative mass spectrometry using label-free quantification nano liquid chromatography tandem mass spectrometry: The samples were re-suspended in 0.1% formic acid and analyzed using label-free quantification nano liquid chromatography tandem mass spectrometry (LFQ nLC-MS/MS). The samples were analyzed in duplicate. LFQ nLC-MS/MS was performed on an Orbitrap Fusion Tribrid mass spectrometer equipped with an EasySpray ion source coupled to a Dionex Ultimate 3000 RSLC nano system (Thermo Fisher Scientific Instruments, Waltham, MA). The sequence in which the samples were run was mixed, thereby distributing the samples from both groups throughout the entire sequence. Technical replicas were run with several days of intermission. Peptides were trapped on a µ-Precolumn (300 µm x 5 mm, C18 PepMap100, 5 µm, 100Å, Thermo Fisher Scientific) and separated on an EASY-spray analytical column (500 mm x 75 µm, PepMap RSCL, C18, 2 mm, 100 Å, Thermo Fisher Scientific).

An elution gradient of 122 min was applied by mixing Buffer A (99.9% water and 0.1% formic acid) and Buffer B (99.9% acetonitrile and 0.1% formic acid). The universal method setting was used to obtain full Orbitrap scans with a scan range (m/z) of 375 to 1,500. The automatic gain control (AGC) target was set to 4×10^5. The maximum injection time was 50 ms. The cycle time was set to 3 s. The most intense precursors with a charge state of 2–7, an intensity threshold of 5×10^3 and a maximum intensity of 1×10^{20} were selected. MS^2 scans were obtained in the linear ion trap in auto-scan range mode with collision-induced dissociation energy at 35%, an AGC target of 2×10^3, and a maximum injection time of 300 ms. Precursor ions were isolated with the quadrupole set using an isolation window of 1.6 m/z. The dynamic exclusion time was 60 s.

LFQ analysis was performed with MaxQuant software [16], Version 1.6.6.0. Files were searched against the UniProt *Homo Sapiens* database downloaded on 19 March, 2021. Carbamidomethyl (C) was used as a fixed modification. Oxidation (M) and acetyl (protein N-terminal) were used as variable modifications. The false discovery rates for PSM, protein, and the site were set to 1%. The LFQ minimum ratio was set to 1. Successful MS/MS was required for LFQ comparisons.

Unique peptides and razor peptides unmodified and modified with oxidation (M) or acetyl (protein N-terminal) were applied for protein quantification. Matching between runs was performed, and a decoy search was performed using revert sequences. Contaminant sequences were included in all searches. The unfiltered results of the database search are provided in Appendix 1.

The MaxQuant output file was entered into Perseus (Version 1.6.2.3) [17]. Only proteins identified by post-translational modification were removed, followed by the removal of proteins identified from a peptide found to be part of a protein derived from the reversed part of the decoy database. Proteins identified as contaminants were also removed from the dataset. Label-free quantification (LFQ) values were $\log_2$ transformed, and mean LFQ values were calculated. For successful protein identification, at least two unique peptides were required. Proteins identified by only one unique peptide were removed from the dataset. All proteins that were successfully identified and quantified are provided in Appendix 2. Before statistical analysis, the proteins were filtered by requiring successful identification and quantification in at least 70% of the samples in the DME group and the control group (Appendix 3). Statistical analysis by Student's t test was performed in Perseus to compare DME with controls. The imputation of missing values was not performed. Corrections for multiple hypothesis testing were executed using the permutation-based method in Perseus [18], with the number of randomizations set to 250 and an S_0 parameter of 0.1. A false discovery rate (FDR) of 0.05 was applied. CST values were $\log_{10}$ transformed before calculating correlations to achieve a normal distribution. Correlations were calculated in STATA 16.0 (StataCorp, College Station, TX) using Pearson's correlation coefficient (r). Correlations were considered statistically significant if $p < 0.05$. STATA 16.0 was used to create scatterplots with predictions from a linear regression.

A gene ontology analysis of Kyoto Encyclopedia of Genes and Genomes (KEGG) pathways regarding regulated proteins was conducted with GeneCodis 4.0 software [19], as previously described [20]. The 10 pathways with the lowest adjusted p values were selected. Cluster analyses were performed with STRING 11.5 (string-db.org) [21–23], as mentioned [13], with the minimum required interaction score set to 0.40 and the MCL inflation parameter set to 3. KEGG pathway analysis was performed in STRING 11.5, with a false discovery rate set to 0.01. Principal component analysis (PCA) was performed in Perseus with default settings after the imputation of missing values from the normal distribution.

Enzyme-linked immunosorbent assay (ELISA): For the quantification of VEGF, the samples were diluted 1:2, and VEGF was quantified as detailed in a previous study using the ab222510 Human VEGF SimpleStep enzyme-linked immunosorbent assay (ELISA) Kit (Abcam, UK) [13]. For the quantification of lipopolysaccharide-binding protein (LBP), the ab279407 Human LBP SimpleStep ELISA® kit (Abcam, UK) was applied, and LBP was quantified according to the manufacturer's instructions. The wash buffer of the kit was diluted at 1:10. The capture and detector antibody solution was diluted at 1:10 in the antibody diluent 4BI of the kit. Standards 1–8 were created with the Sample Diluent NS of the kit. The samples were centrifuged at 2,000 × *g* for 10 min and diluted 1:500 in the Sample Diluent NS of the kit. A volume of 50 µl sample or standard was added to the appropriate wells, and 50 µl of the antibody solution was added to each well. The plate was sealed and incubated for 60 min at room temperature on a plate shaker set to 400 rpm. The wells were washed three times with 350 µl wash buffer. A volume of 100 µl TMB Development Solution was added to each well, followed by incubation in the dark for 10 min on a plate shaker set to 400 rpm. A volume of 100 µl Stop Solution of the kit was added. The plate was shaken on a plate shaker for 1 min. The optical density was recorded at 450 nm. Quantitative data were $\log_{10}$ transformed to obtain a normal distribution. ELISA assays were performed in duplicate for all samples and standards. The average of duplicate readings for each standard and sample was calculated, and the average zero standard optical density was subtracted. Subsequently, sample values were normalized by determining the ratio of the sample absorbance to the absorbance of the standards, ensuring a standardized comparison across all samples. Statistical analyses of the ELISA data were conducted using the Student's *t* test and Pearson's correlation coefficient (r). Differences and correlations were considered statistically significant if $p < 0.05$ [13].

Immunofluorescence: Human postmortem eyes were provided by Corneabank, Beverwijk, the Netherlands. All procedures were in accordance with the provisions of the Declaration of Helsinki for the use of human tissue in research. A 61-year-old female with diabetic retinopathy treated with laser with more than 12 years of Type-2 diabetes and insulin use and a 68-year-old female non-diabetic patient were selected. The postmortem delays were 13 and 17 h, respectively. The semiquantitative grading of PAL-E on the vascular endothelium depicted patchy to uniformly marked staining [24] in two independent sections of the donor with diabetic retinopathy. Sections of 10 µm thickness were cut and fixed in 4% (w/v) formaldehyde for 20 min and were washed once in 3x phosphate-buffered saline (PBS). Individual sections were encircled using a PAP pen to form a hydrophobic barrier. The sections were incubated for 1 h in 1x PBS supplemented

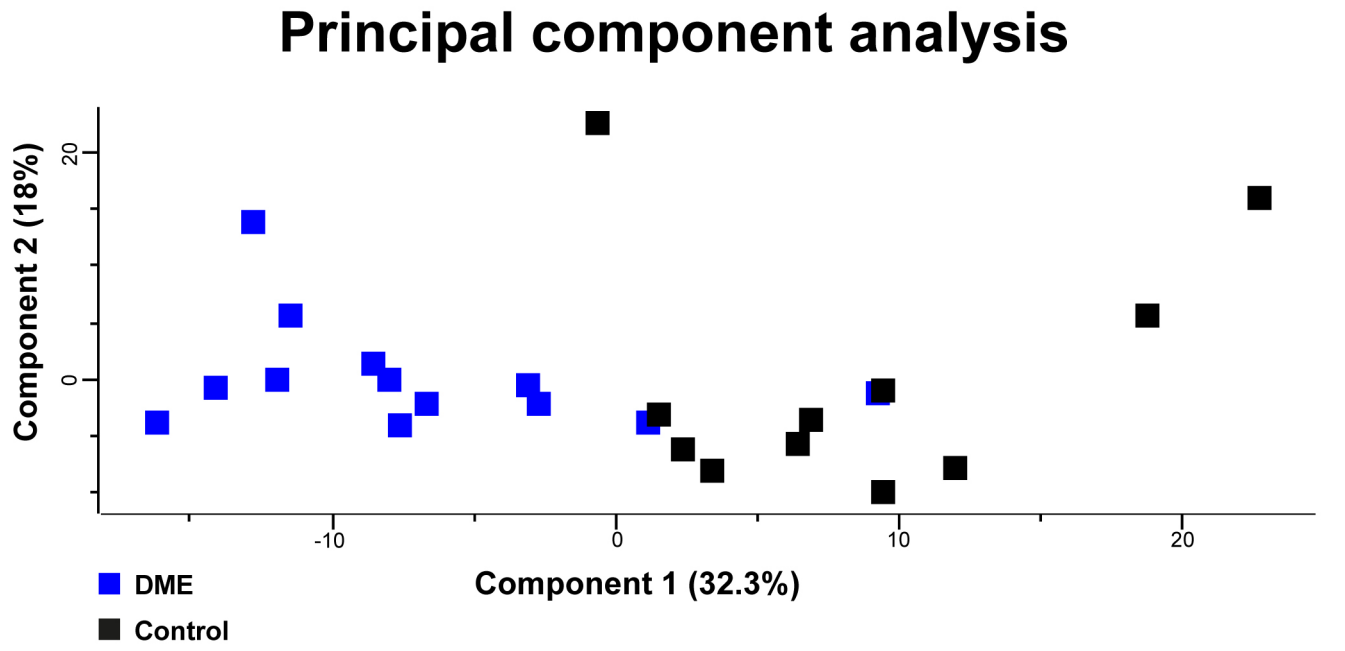

Figure 1. Principal component analysis (PCA). The PCA analysis indicated that DME samples could generally be separated from control samples based on the proteomes, as there was little overlap between DME and control samples.

with 10% normal goat serum and 0.1% Triton X-100. Next, the slides were washed three times with PBS and incubated overnight at 4 °C with anti-human monoclonal mouse antibody PAL-E (Pathologische Anatomie Leiden–Endothelium; 1:200) and fluorescein isothiocyanate (FITC)-conjugated polyclonal rabbit anti-human fibrinogen (F0111, DAKO; 1:200). Antibodies were diluted in normal antibody diluent (AB999, Scytek). Sections were subsequently washed three times with PBS and incubated with goat anti-mouse Alexa Fluor™ 633 antibody (A21052, Life Technologies; 1:100). The sections were again washed three times with PBS and mounted with Vectashield antifade mounting medium with DAPI (H-1200–10, Vector Laboratories). Sections were imaged using a confocal laser scanning microscope (Leica, SP8) with settings kept constant between conditions.

RESULTS

Proteome analysis of diabetic macular edema (DME): Proteome analysis was performed on aqueous humor samples from patients with treatment-naïve DME and age-matched controls. A total of 891 proteins were successfully identified in the combined set of aqueous samples (Supporting Data Values S1). In total, 256 aqueous humor proteins were successfully identified and quantified in at least 70% of the samples in each group (Supporting Data Values S2), and statistical analysis was performed on these proteins.

In the PCA plot, DME samples could generally be separated from control samples based on their proteomes (Figure 1). After correction for multiple hypothesis testing, 101 proteins were statistically significantly regulated in the DME group compared to the controls (Table 3; Figure 2). Among the significantly regulated proteins, 55 proteins were increased in content in DME, and 46 proteins were decreased in content (Table 3; Figure 2).

Bioinformatics: The proteins regulated in DME were associated with complement and coagulation cascades, glycolysis/gluconeogenesis, cholesterol metabolism, pyruvate metabolism, ECM-receptor interaction, hypoxia inducible factor-1 (HIF-1) signaling, carbon metabolism, and glucagon signaling (Figure 3A,B). Among the regulated proteins, a large cluster of proteins was formed by proteins involved in complement and coagulation cascades (Figure 3B). STRING cluster analysis also identified a major cluster of proteins involved in complement and coagulation cascades (Figure 4A), which were all increased in content. Proteins involved in complement and coagulation cascades included complement factors (C2, C3, C4B, C5, C6, C7, C8A, C8G, C9, and CFH), fibrinogen chains (FGA, FGB, and FGG), vitronectin (VTN), alpha-1-antitrypsin (SERPINA1), antithrombin-III (SERPINC1), heparin cofactor 2 (SERPIND1), alpha-2-antiplasmin (SERPINF1), plasma kallikrein (KLKB1),

Table 3. Significantly regulated proteins ordered according to fold change.

Protein ID	Protein names	Gene names	p-value	Fold change DME/control
P02671	Fibrinogen alpha chain	FGA	1.49×10^{-6}	17.8
P02675	Fibrinogen beta chain	FGB	8.19×10^{-7}	15.8
P02679	Fibrinogen gamma chain	FGG	2.26×10^{-7}	12.2
P02656	Apolipoprotein C-III	APOC3	0.000177	6.40
P00738	Haptoglobin	HP	0.054	3.81
P18428	Lipopolysaccharide-binding protein	LBP	1.3×10^{-8}	3.65
P06727	Apolipoprotein A-IV	APOA4	1.03×10^{-6}	3.56
P02751	Fibronectin	FN1	2.5×10^{-6}	2.96
P06312	Ig kappa chain V-IV region	IGKV4–1	0.0025	2.95
P02760	Protein AMBP	AMBP	0.0017	2.85
Q14624	Inter-alpha-trypsin inhibitor heavy chain H4	ITIH4	3.45×10^{-5}	2.71
P02750	Leucine-rich alpha-2-glycoprotein	LRG1	0.0022	2.52
P02647	Apolipoprotein A-I	APOA1	0.00064	2.51
P19827	Inter-alpha-trypsin inhibitor heavy chain H1	ITIH1	9.84×10^{-5}	2.42
P01031	Complement C5	C5	0.00051	2.41
P27169	Serum paraoxonase/arylesterase 1	PON1	0.00059	2.38
P01876	Ig alpha-1 chain C region	IGHA1	6.19×10^{-5}	2.34
P19823	Inter-alpha-trypsin inhibitor heavy chain H2	ITIH2	0.00014	2.29
P04004	Vitronectin	VTN	0.00040	2.29
P00734	Prothrombin	F2	0.0080	2.16
P08603	Complement factor H	CFH	0.00014	2.12
P05546	Heparin cofactor 2	SERPIND1	0.00055	2.11
P08697	Alpha-2-antiplasmin	SERPINF2	0.0017	2.09
P0C0L5	Complement C4-B	C4B	0.0032	2.06
P02748	Complement component C9	C9	0.015	2.04
A0A075B6J9		IGLV2–18	0.0044	2.03
P01042	Kininogen-1	KNG1	0.00074	1.92
P04180	Phosphatidylcholine-sterol acyltransferase	LCAT	0.0041	1.92
P01024	Complement C3	C3	6.02×10^{-5}	1.90
P01008	Antithrombin-III	SERPINC1	0.0015	1.90
P03952	Plasma kallikrein	KLKB1	0.0029	1.89
P10643	Complement component C7	C7	0.0021	1.88
P13671	Complement component C6	C6	0.0019	1.87
P07360	Complement component C8 gamma chain	C8G	0.0054	1.84
P04432	Ig kappa chain V-I region Daudi	IGKV1–12	0.045	1.78
P25311	Zinc-alpha-2-glycoprotein	AZGP1	0.00054	1.78
P01011	Alpha-1-antichymotrypsin	SERPINA3	0.0041	1.77
P08185	Corticosteroid-binding globulin	SERPINA6	0.011	1.75
P05543	Thyroxine-binding globulin	SERPINA7	0.021	1.75
P43652	Afamin	AFM	0.018	1.75
P01009	Alpha-1-antitrypsin	SERPINA1	0.0014	1.74

Protein ID	Protein names	Gene names	p-value	Fold change DME/control
P06681	Complement C2	C2	0.0037	1.70
P26927	Hepatocyte growth factor-like protein	MST1	0.0056	1.68
P02753	Retinol-binding protein 4	RBP4	0.0051	1.68
P04217	Alpha-1B-glycoprotein	A1BG	0.0095	1.65
P51884	Lumican	LUM	0.0015	1.55
P07357	Complement component C8 alpha chain	C8A	0.012	1.54
Q96PD5	N-acetylmuramoyl-L-alanine amidase	PGLYRP2	0.019	1.54
P08571	Monocyte differentiation antigen CD14	CD14	0.00066	1.54
P01023	Alpha-2-macroglobulin	A2M	0.016	1.53
P01019	Angiotensinogen	AGT	0.014	1.50
P0DOY3	Ig lambda-6 chain C region	IGLC6	0.0067	1.48
P04196	Histidine-rich glycoprotein	HRG	0.019	1.44
P02790	Hemopexin	HPX	0.013	1.39
P00450	Ceruloplasmin	CP	0.00096	1.35
Q96KN2	Beta-Ala-His dipeptidase	CNDP1	0.024	0.66
Q92520	Protein FAM3C	FAM3C	0.012	0.64
Q14118	Dystroglycan	DAG1	0.037	0.60
P23471	Receptor-type tyrosine-protein phosphatase zeta	PTPRZ1	0.010	0.60
Q9HCB6	Spondin-1	SPON1	0.019	0.60
P13591	Neural cell adhesion molecule 1	NCAM1	0.0063	0.60
P08294	Extracellular superoxide dismutase [Cu-Zn]	SOD3	0.026	0.60
P07195	L-lactate dehydrogenase B chain	LDHB	0.038	0.59
Q9BU40	Chordin-like protein 1	CHRDL1	0.0060	0.59
Q12860	Contactin-1	CNTN1	0.024	0.58
Q12805	EGF-containing fibulin-like extracellular matrix protein 1	EFEMP1	0.0042	0.57
Q92823	Neuronal cell adhesion molecule	NRCAM	0.012	0.56
Q9UHL4	Dipeptidyl peptidase 2	DPP7	0.0040	0.55
Q86UX2	Inter-alpha-trypsin inhibitor heavy chain H5	ITIH5	0.048	0.52
P10599	Thioredoxin	TXN	0.013	0.52
P35555	Fibrillin-1	FBN1	0.011	0.52
Q9Y4C0	Neurexin-3	NRXN3	0.0038	0.52
Q08554	Desmocollin-1	DSC1	0.038	0.51
P31025	Lipocalin-1	LCN1	0.048	0.51
Q06481	Amyloid-like protein 2	APLP2	0.028	0.50
Q14767	Latent-transforming growth factor beta-binding protein 2	LTBP2	0.0035	0.50
Q9P121	Neurotrimin	NTM	0.0052	0.50
P30086	Phosphatidylethanolamine-binding protein 1	PEBP1	6.77×10^{-5}	0.49
P98164	Low-density lipoprotein receptor-related protein 2	LRP2	0.025	0.49
P98160	Basement membrane-specific heparan sulfate proteoglycan core protein	HSPG2	0.030	0.47

Protein ID	Protein names	Gene names	p-value	Fold change DME/control
P62987	Ubiquitin-60S ribosomal protein L40	UBA52	0.0061	0.45
Q08629	Testican-1	SPOCK1	0.014	0.45
P06733	Alpha-enolase	ENO1	0.012	0.44
P09972	Fructose-bisphosphate aldolase C	ALDOC	0.0013	0.42
Q08380	Galectin-3-binding protein	LGALS3BP	0.037	0.41
P00338	L-lactate dehydrogenase A chain	LDHA	0.030	0.41
P78509	Reelin	RELN	0.052	0.39
P14618	Pyruvate kinase PKM	PKM	0.0027	0.38
P07737	Profilin-1	PFN1	0.012	0.38
Q02413	Desmoglein-1	DSG1	0.0029	0.37
P23528	Cofilin-1	CFL1	0.054	0.36
O00468	Agrin	AGRN	0.00097	0.34
P11021	78 kDa glucose-regulated protein	HSPA5	0.032	0.34
Q9NZT1	Calmodulin-like protein 5	CALML5	0.058	0.30
P31151	Protein S100-A7	S100A7	0.043	0.29
P00558	Phosphoglycerate kinase 1	PGK1	0.00026	0.25
P63104	14–3-3 protein zeta/delta	YWHAZ	0.010	0.24
P22914	Beta-crystallin S	CRYGS	0.0060	0.23
P04075	Fructose-bisphosphate aldolase A	ALDOA	0.00062	0.19
P15924	Desmoplakin	DSP	0.014	0.18
P48594	Serpin B4	SERPINB4	0.040	0.12

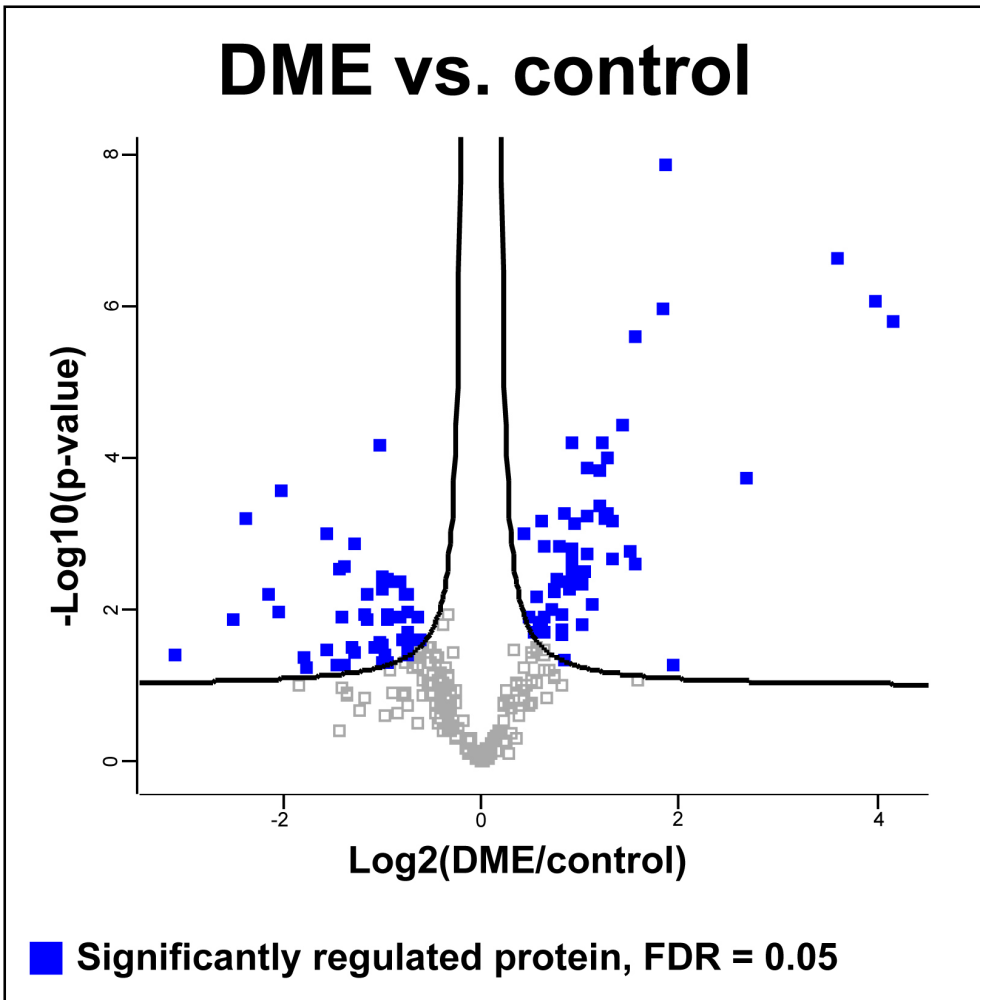

Figure 2. Volcano plot. Log_2 transformed abundance ratios for each protein are plotted on the x-axis. Negative log_{10} transformed p values are plotted on the y-axis. A false discovery rate (FDR) of 0.05 was applied. Statistically significantly regulated proteins are localized above the full curves. A total of 101 proteins were significantly regulated in the DME group compared to the controls (blue squares).

kininogen-1 (KNG1), alpha-2-macroglobulin (A2M), and prothrombin (F2).

DME was associated with the regulation of a cluster of proteins involved in ECM–receptor interaction, including agrin, basement membrane-specific heparan sulfate proteoglycan core protein (HSPG2), dystroglycan, and fibronectin (Figure 4A). Fibronectin was upregulated in DME, whereas agrin, dystroglycan, and HSPG2 were downregulated.

Another cluster of regulated proteins contained proteins involved in cholesterol metabolism, including apolipoprotein A-I (APOA1), apolipoprotein C-III (APOC3), apolipoprotein A-IV (APOA4), low-density lipoprotein receptor-related protein 2 (LRP2), and phosphatidylcholine-sterol acyltransferase (LCAT; Figure 4A). All lipoproteins and phosphatidylcholine-sterol acyltransferase were increased in DME, while lipoprotein receptor-related protein 2 was downregulated. STRING cluster analysis discerned a cluster of regulated proteins that represented multiple KEGG pathways (Figure 4B–F). The proteins of this cluster were downregulated and included alpha-enolase (ENO1), fructose-bisphosphate aldolase A (ALDOA), fructose-bisphosphate aldolase C (ALDOC), L-lactate dehydrogenase A chain (LDHA), L-lactate dehydrogenase B chain (LDHB), phosphoglycerate kinase 1 (PGK1), and pyruvate kinase PKM (PKM). The regulation of these proteins indicates that DME was associated with the regulation of the carbon metabolism, the HIF-1 signaling pathway, the glucagon signaling pathway, the pyruvate metabolism, and glycolysis/ gluconeogenesis (Figure 4B–F).

Correlations with clinical parameters: Positive correlations with BCVA were observed for complement C2, complement C5, complement C8 alpha chain, fibronectin, hepatocyte growth factor-like protein, and zinc-alpha-2-glycoprotein. Negative correlations with BCVA were observed for 78 kDa glucose-regulated protein, amyloid-like protein 2,

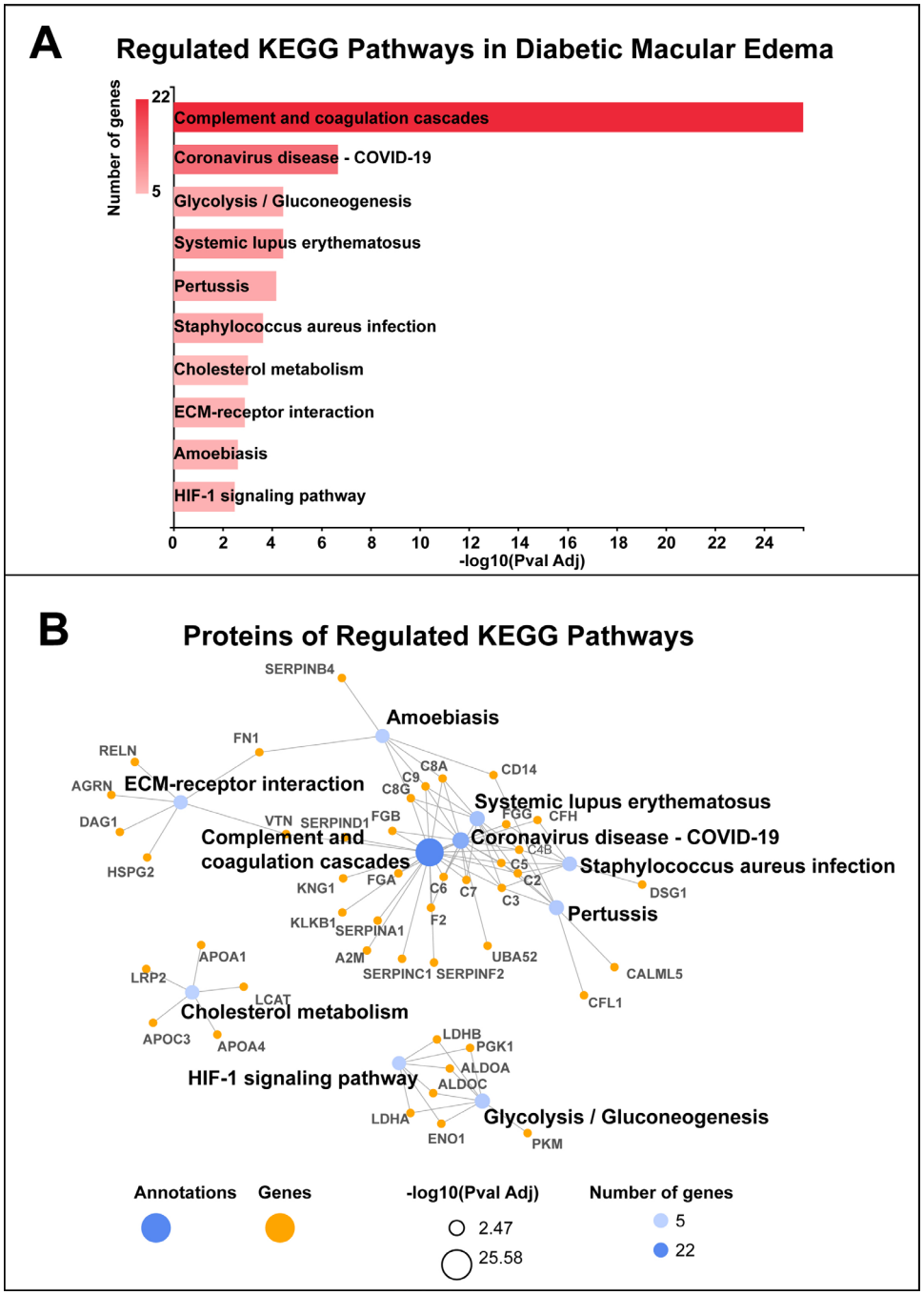

Figure 3. Pathway analysis**. A:** KEGG pathway analysis of regulated proteins performed in GeneCodis 4.0. Significantly regulated proteins were involved in complement and coagulation cascades, glycolysis/ gluconeogenesis, cholesterol metabolism, ECM-receptor interaction, and the HIF-1 signaling pathway. **B:** A large group of proteins were involved in complement and coagulation cascades, including complement factors (C2, C3, C4B, C5, C6, C7, C8A, C8G, C9, and CFH), fibrinogen chains (FGA, FGB, and FGG), vitronectin (VTN), alpha-1-antitrypsin (SERPINA1), antithrombin-III (SERPINC1), heparin cofactor 2 (SERPIND1), alpha-2-antiplasmin (SERPINF1), plasma kallikrein (KLKB1), kininogen-1 (KNG1), alpha-2-macroglobulin (A2M), and prothrombin (F2).

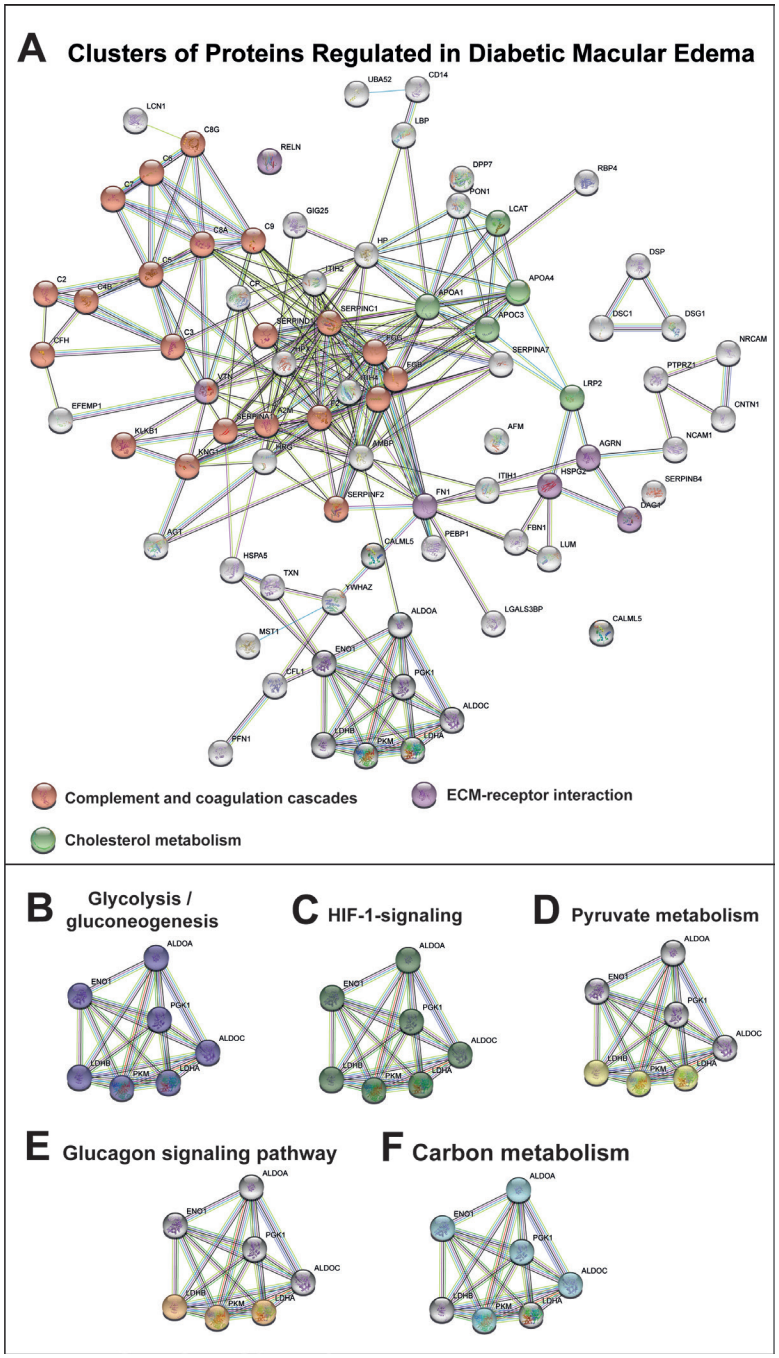

Figure 4. STRING cluster analysis of regulated proteins in DME. **A:** A large cluster was formed by proteins involved in complement and coagulation cascades, including complement factors (C2, C3, C4B, C5, C6, C7, C8A, C8G, C9, and CFH), fibrinogen chains (FGA, FGB, and FGG), vitronectin (VTN), alpha-1-antitrypsin (SERPINA1), antithrombin-III (SERPINC1), heparin cofactor 2 (SERPIND1), alpha-2-antiplasmin (SERPINF1), plasma kallikrein (KLKB1), kininogen-1 (KNG1), alpha-2-macroglobulin (A2M), and prothrombin (F2). Another cluster was involved in ECM–receptor interaction, including agrin (AGRN), fibronectin (FN1), dystroglycan (DAG1), and basement membrane-specific heparan sulfate proteoglycan core protein (HSPG2). A third cluster of proteins was involved in the cholesterol metabolism, including apolipoprotein A-I (APOA1), apolipoprotein C-III (APOC3), apolipoprotein A-IV (APOA4), low-density lipoprotein receptor-related protein 2 (LRP2), and phosphatidylcholine-sterol acyltransferase (LCAT). **B**–**F:** A cluster of proteins represented multiple KEGG pathways. This was the case for fructose-bisphosphate aldolase C (ALDOC), fructose-bisphosphate aldolase A (ALDOA), alpha-enolase (ENO1), phosphoglycerate kinase 1 (PGK1), L-lactate dehydrogenase A chain (LDHA), L-lactate dehydrogenase B chain (LDHB), and pyruvate kinase PKM (PKM). The regulation of these proteins suggests that DME was associated with glycolysis/gluconeogenesis, the pyruvate metabolism, the carbon metabolism, HIF signaling, and the glucagon signaling pathway.

beta-crystallin S, low-density lipoprotein receptor-related protein 2, neurexin-3, and testican-1 (Figure 5).

Positive correlations with CST were observed for ceruloplasmin and the complement component C8 alpha chain (Figure 6). Negative correlations with CST were observed for desmocollin-1, desmoglein-1, and dipeptidyl peptidase 2 (Figure 6).

Validation by ELISA: Mass spectrometry identified an increased level of LBP in DME (fold change = 3.65; p = 1.3×10^{-8}; Figure 7A). The upregulation of LBP in DME was

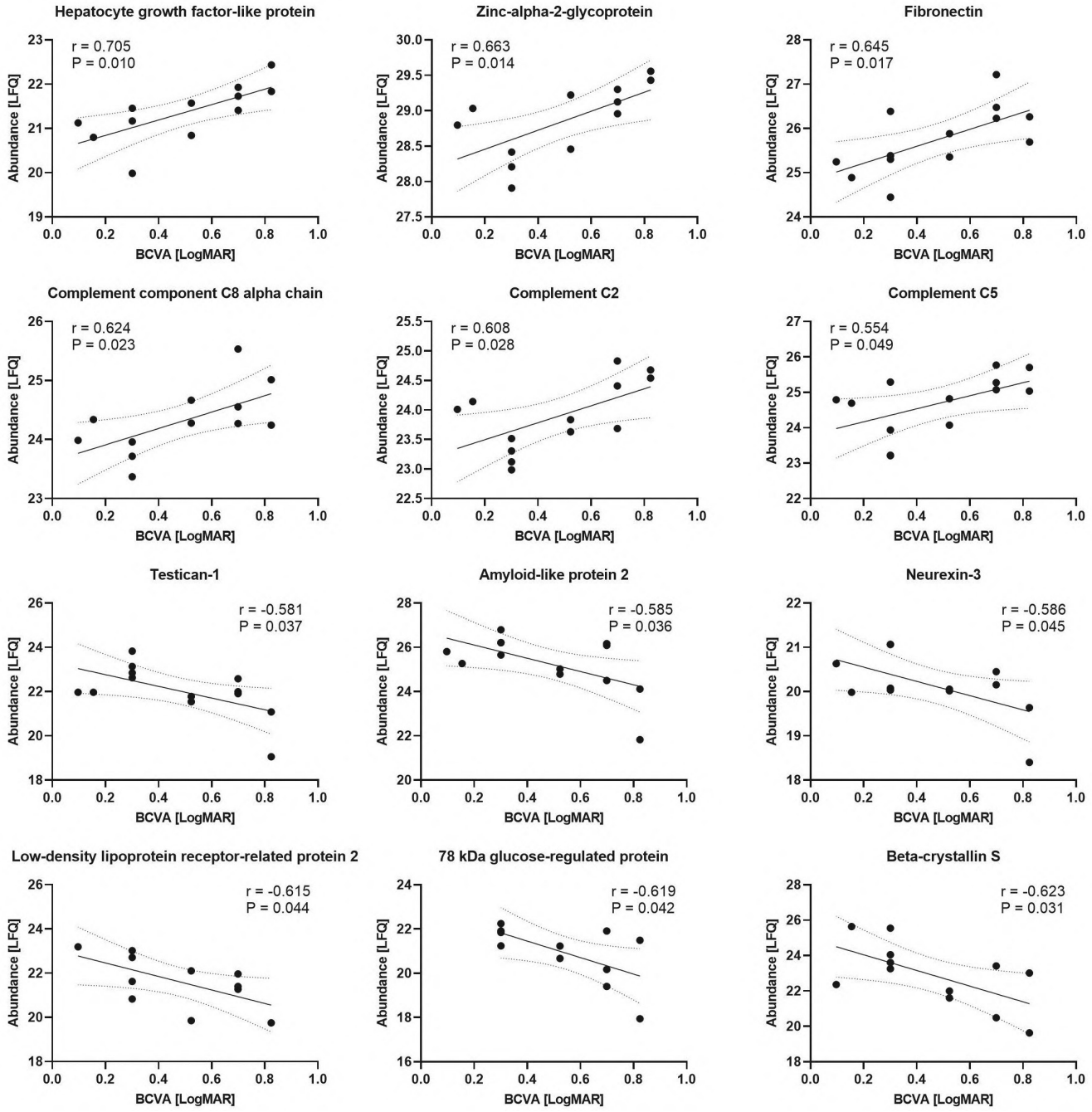

Figure 5. Correlation plots of protein levels strongly correlated with BCVA. All data points of the relative abundance of protein levels as determined by mass spectrometry are plotted against the corresponding BCVA values of each patient. A best-fit linear regression line with 95% confidence bands (dotted line) is shown. Protein levels are presented as $\log_2$-transformed label-free quantification units (LFQ); BCVA values are $\log_{10}$-transformed. Pearson's correlation coefficient (r) and p values (P) are given, with $p < 0.05$ being statistically significant.

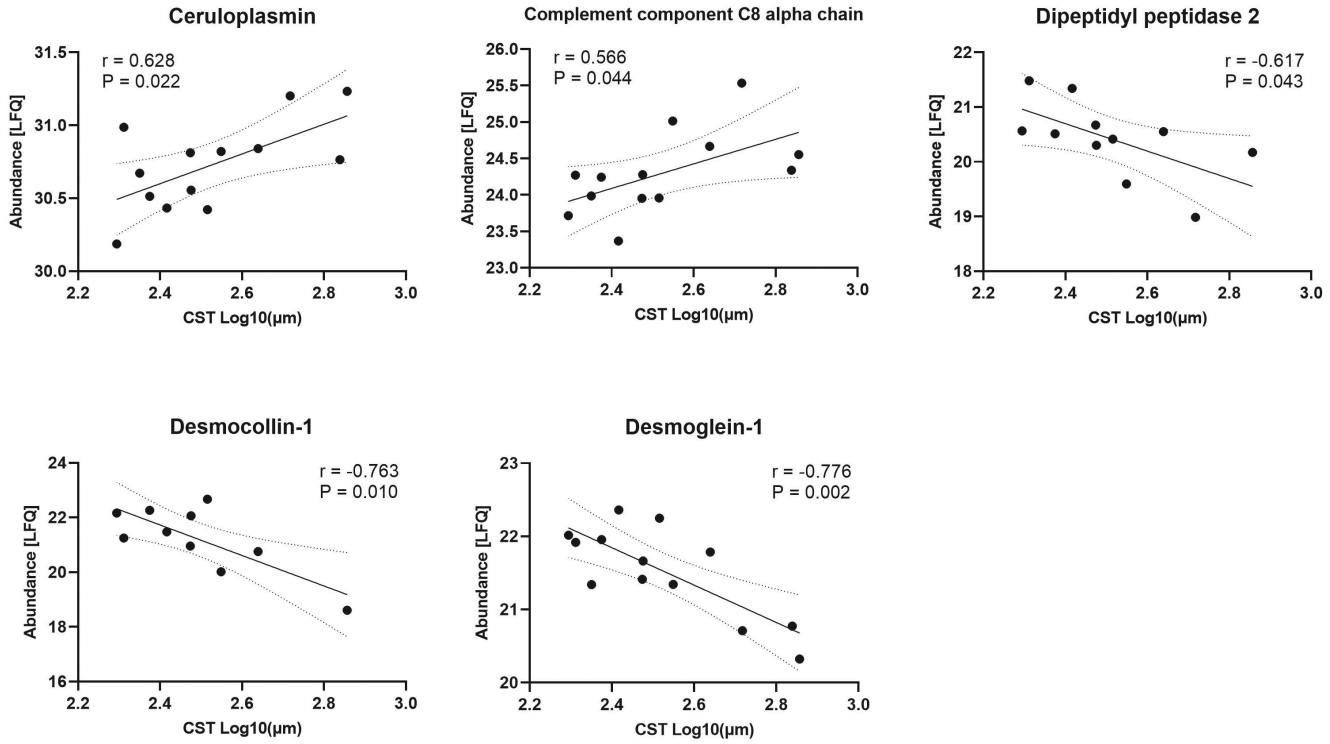

Figure 6. Correlation plots of protein levels correlated with CST. All data points of the relative abundance of protein levels as determined by mass spectrometry are plotted against the corresponding CST values of each patient. A best-fit linear regression line with 95% confidence bands (dotted line) is shown. Protein levels are presented as log_2-transformed label-free quantification units (LFQ); CST values are log_{10}-transformed. Pearson's correlation coefficient (r) and p values (P) are given, with $p < 0.05$ being statistically significant.

confirmed by ELISA, thereby validating the proteomic analysis (fold change = 1.72; p = 0.048; Figure 7A). VEGF was significantly increased in DME (p = 0.015; Figure 7A). LBP correlated significantly with VEGF (r = 0.68; p = 0.0077; Figure 7B). LBP quantified with mass spectrometry correlated with CST (r = 0.59; p = 0.035). Nonetheless, the correlation was not confirmed by ELISA (r = 0.31; p = 0.27; Figure 7B).

Immunofluorescence: To illustrate the involvement of fibrinogen extravasation in DME, we performed immunostainings on human retinal tissue sections of DR patients and non-diabetic controls. As an indicator of blood–retinal barrier breakdown, we used the monoclonal antibody PAL-E [25], which recognizes plasmalemma vesicle-associated protein (PLVAP), which is crucially involved in DME [28]. The semiquantitative grading of PAL-E on the vascular endothelium revealed patchy to uniformly marked staining [24] in independent sections of the DR donor. The co-localization of PLVAP with the extravasation of fibrinogen was observed in DME, whereas fibrinogen in the non-diabetic control was more confined within blood vessels (Figure 8).

DISCUSSION

More than 100 proteins were regulated in DME, supporting a multifactorial pathogenesis. This multifaceted protein-driven response highlights the importance of considering alternative therapies in cases of an inadequate response to anti-VEGF agents. Strategies to address the multifactorial response include anti-VEGF therapy combined with navigated central laser [7] and dexamethasone intravitreal implants [26]. Some degree of variation was observed in the DME samples (Figure 1). DME may occur at any stage of diabetic retinopathy [27]. Some of the observed variation may be ascribed to the fact that DME can occur at all stages of diabetic retinopathy. The DME phenotype in this donor was defined by a high PAL-E score, indicative of blood–retinal barrier breakdown [24,25,28]. These immunofluorescent stainings of fibrinogen in a donor with DME are consistent with the increased protein concentration observed in the aqueous humor. In retinal vascular diseases, intraocular fibrinogen is associated with retinal ischemia and may be considered a marker of the severity of retinal vascular disease. Furthermore, fibrinogen extravasation is an acknowledged phenomenon of DME

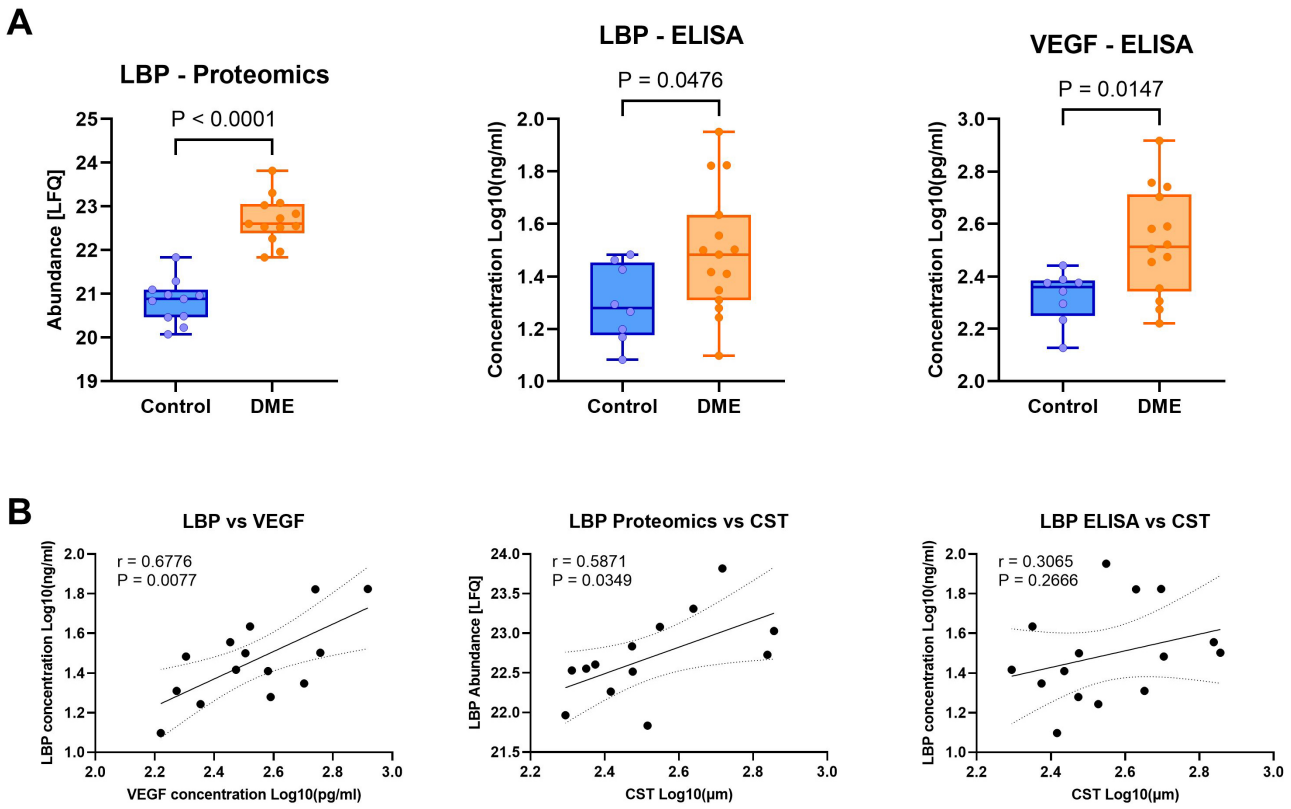

Figure 7. LBP and VEGF protein levels in DME and their correlations with CST. **A:** Relative abundance of LBP protein as determined by proteomic analysis using mass spectrometry expressed in $\log_2$-transformed label-free quantification units (LFQ), and LBP and VEGF $\log_{10}$-transformed concentrations as determined by ELISA. **B:** Correlation between LBP and VEGF concentrations, correlation between LBP proteomics data and CST, and correlation between LBP protein concentrations of ELISA and CST. A best-fit linear regression line with 95% confidence bands (dotted line) is shown. Pearson's correlation coefficient (r) and p values (P) are given, with $p < 0.05$ being statistically significant.

[25]. In BRVO and CRVO, fibrinogen correlates with visual acuity and the severity of macular edema [13,14]. Fibrinogen plays essential roles in coagulation, inflammation, and tissue repair [29]. Fibrinogen was upregulated in the endothelium of the retinal vessels and in proximity to the vessels in DME, indicating involvement in the disruption of the blood–retinal barrier.

The number of proteins that correlated with BCVA was higher than the number of proteins that correlated with CST, suggesting that some proteins contribute to visual loss regardless of the severity of the edema. Proteins associated with loss of visual function without a relationship to the severity of DME are likely to be associated with macular ischemia.

Our study identified several proteins that are not traditionally associated with DME. The elevated aqueous contents of the pro-inflammatory proteins LBP and CD14 were observed in DME. LBP and CD14 have regulatory functions in the innate immune system, whereby both proteins are involved in the recognition of lipopolysaccharide, the major component of the outer membrane of Gram-negative bacteria. LBP brings lipopolysaccharides to the cellular surface of monocytes, where it forms a complex with CD14 [30,31]. LBP correlated with VEGF, indicating an interaction between the two proteins. We previously identified increased levels of LBP and CD14 in the aqueous humor of patients with BRVO [13]. In DME, the fold change in LBP was 3.65 compared to 1.48 in BRVO [13], indicating that the inflammatory response is particularly pronounced in DME.

Future studies should address the associations between LBP and CD14 and the most important challenges in the management of DME, which include the recurrence of macular edema and a poor response to anti-VEGF therapy [6]. The roles of key proteins identified in our study warrant further exploration in animal models of retinal vascular disease. For example, LBP knockout models protect against inflammation through decreased neutrophil infiltration and

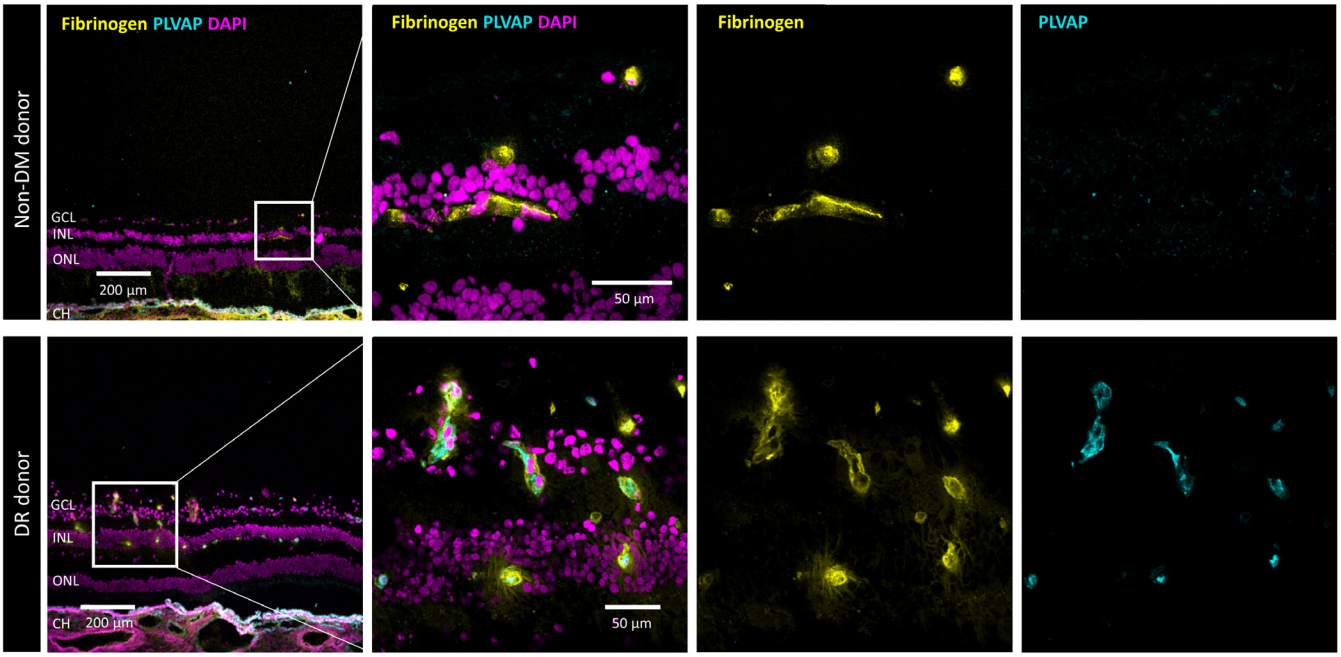

Figure 8. Immunofluorescence staining of fibrinogen in the human retina. Representative confocal images of human retinal cryosections from non-diabetic (DM) donors (upper panel) and donors with diabetic retinopathy (DR; lower panel), immunolabeled for fibrinogen (yellow) and PLVAP (cyan). Nuclei were stained with DAPI (magenta). Higher magnifications of the retina reveal the co-localization of fibrinogen and PLVAP, as well as separate channels for fibrinogen and PLVAP. CH, choroid; GCL, ganglion cell layer; INL, inner nuclear layer; ONL, outer nuclear layer.

oxidative stress [32]. However, how LBP knockout models respond to retinal vascular disease remains to be studied. A relevant approach would be to expose LBP knockout models to experimental retinal vascular disease, such as retinal ischemia [33] or retinal vein occlusion [20].

A cluster of proteins involved in ECM–receptor interaction was identified in DME, including agrin, HSPG2, dystroglycan, and fibronectin. HSPG2 is predominantly expressed in the basal membrane of retinal vessels and in Bruch's membrane [34]. The regulation of HSPG2 in DME reflects changes in the basal membrane, which are likely associated with increased vascular permeability in DME. HSPG2 has angiogenic and anti-angiogenic features [35]. However, our study does not provide details about whether the angiogenic or antiangiogenic features of HSPG2 are activated in DME. Dystroglycan is strongly expressed around retinal vessels and provides structural integrity for the retina [36,37]. Nonetheless, its role in DME warrants further investigation.

Fibronectin was previously found to correlate with BCVA in BRVO and CRVO [13,14]. Here, we found a similar correlation in DME. The soluble form of fibronectin, a 230 to 270 kDa glycoprotein, is known to regulate thrombosis and accelerate wound healing [38–40]. We have previously shown that fibronectin is associated with retinal ischemia in retinal vascular disease [13], which is also likely the case in diabetic retinopathy.

A large cluster of upregulated complement factors was identified in DME. The complement component C8 alpha chain correlated with BCVA and CST, while complement C2 and complement C5 correlated with BCVA. Complement components may contribute to the inflammatory response in DME. Retinal complement factors increase in content under ischemic conditions in animal models of experimental retinal vascular disease [12]. An association between aqueous complement C5 and clinical parameters, including the severity of macular edema and retinal ischemia, has previously been reported in retinal vascular disease [13]. Indeed, the role of complement C5 in ischemic changes in diabetic retinopathy may be considered.

The strongest correlation with BCVA was observed for hepatocyte growth factor-like protein, a liver-derived serum glycoprotein involved in cell proliferation and differentiation. Hepatocyte growth factor-like protein is synthesized by hepatocytes and has a variety of functions, including growth, morphogenesis, and the recruitment of macrophages [41–43].

Nevertheless, its role in retinal vascular disease remains largely unstudied.

Negative correlations with CST were observed for desmocollin-1 and desmoglein-1, both of which are involved in desmosomal integrity. Desmoglein-1 and desmocollin-1 are desmosomal cadherins that form stable associations with similar cadherins in adjacent cells [44]. The loss of desmoglein-1 was previously reported in brain endothelium exposed to oxidative stress, suggesting alterations in the blood–brain barrier [45]. Future studies may investigate whether the downregulation of desmoglein-1 and desmocollin-1 in DME leads to the disruption of the blood–retinal barrier.

Moreover, dipeptidyl peptidase 2, which correlated negatively with CST, is an intracellular protease localized in the vesicular system of the cytosol [46]. Dipeptidyl peptidase 2 knockout mice present with hyperinsulinemia, impaired glucose intolerance, insulin resistance, and visceral obesity [47]. The data from our study indicate that dipeptidyl peptidase 2 may have a protective effect on DME.

An increased level of the acute-phase reactant hemopexin was observed in DME. Our results corroborate the findings reported by Hernández et al. [48], who identified increased levels of hemopexin in vitreous samples from patients with DME and suggested that hemopexin is involved in processes leading to the disruption of the blood–retinal barrier.

Gao et al. [49] observed increased levels of antithrombin III and prothrombin in vitreous samples from patients with diabetic retinopathy and suggested that these proteins are involved in thrombosis and inflammation, leading to increased vascular permeability in DME. Several apolipoproteins were increased in DME, including apolipoprotein A-I, apolipoprotein A-IV, and apolipoprotein C-III. These apolipoproteins were previously reported to be upregulated in vitreous samples from patients with DME and are thought to contribute to the deposition of hard exudates [9]. In DME, we identified an increased level of plasma kallikrein, a circulating component of innate inflammation. Clermont et al. [50] previously demonstrated that VEGF-induced retinal vascular permeability and retinal thickening are reduced in plasma prekallikrein-deficient mice and plasma kallikrein inhibitors are emerging as therapies against DME [51].

DME was associated with the downregulation of the proteins of the glycolytic pathway, including fructose-bisphosphate aldolases A and C, alpha-enolase, phosphoglycerate kinase 1, pyruvate kinase, L-lactate dehydrogenase A chain, and L-lactate dehydrogenase B chain. The regulation of glycolysis under hypoxic conditions is followed by the upregulation of glycolytic enzymes promoted by HIF with greater flow through the glycolytic pathway [52]. Therefore, it is highly intriguing that the enzymes of the glycolytic pathway were downregulated in DME compared to the controls. The downregulation of glycolytic enzymes in DME may reflect alterations to glycolytic homeostasis, and the role of the glycolytic pathway in DME warrants further study. Furthermore, the downregulation of glycolytic enzymes highlights the need for tight glycemic control.

In conclusion, our findings support the multifactorial pathogenesis of DME driven by several proteins with a variety of functions. Immunofluorescence staining for fibrinogen showed good consistency between aqueous humor protein changes and protein changes at the retinal level. Increased levels and significant correlations with BCVA were observed for complement components C2, C5, C8, fibronectin, and hepatocyte growth factor-like protein, which were upregulated in DME and correlated with BCVA. Complement C8 and ceruloplasmin were upregulated and correlated with CST. LBP was upregulated in DME and correlated with VEGF. In conclusion, our data are consistent with a multi-faceted inflammatory response in DME. The proteins involved in desmosomal integrity, including desmocollin-1 and desmoglein-1, were downregulated and correlated negatively with CST. Decreased levels were observed in the basal membrane proteins dystroglycan and heparan sulfate proteoglycan core protein. Changes in desmosomal and basal membrane proteins are likely to reflect changes in the integrity of the blood–retinal barrier. Multiple proteins of the glycolytic pathway were downregulated in DME. While the downregulation of glycolytic proteins is not completely understood, it highlights the importance of glycemic control in the development of DME.

APPENDIX 1. SUPPLEMENTAL MATERIAL DATA SETS 1.

To access the data, click or select the words "Appendix 1." Unfiltered results of database search.

APPENDIX 2. SUPPLEMENTAL MATERIAL DATA SETS 2.

To access the data, click or select the words "Appendix 2." All successfully identified proteins.

APPENDIX 3. SUPPLEMENTAL MATERIAL DATA SETS 3.

To access the data, click or select the words "Appendix 3." Proteins identified and quantified in at least 70% of the samples in each group.

ACKNOWLEDGMENTS

The authors thank Mona Britt Hansen, Aarhus University, Aarhus, Denmark, for her expert technical assistance. Financial support: The authors thank Fight for Sight Denmark, Helene og Viggo Bruuns Fond, the Svend Andersen Foundation, Synoptik-Fonden, the Herta Christensen Foundation, the North Denmark Region (2013–0076797), Speciallæge Heinrich Kopps Legat, the Danish Society of Ophthalmology, and Overlægerådets Forskningsfond, Odense University Hospital, Odense, Denmark, for their generous support. The mass spectrometers used for the study were funded by A.P. Møller og Hustru Chastine Mc-Kinney Møllers Fond til almene Formaal.

REFERENCES

1. Starace V, Battista M, Brambati M, Cavalleri M, Bertuzzi F, Amato A, Lattanzio R, Bandello F, Cicinelli MV. The role of inflammation and neurodegeneration in diabetic macular edema. Ther Adv Ophthalmol 2021; 13:25158414211055963[PMID: 34901746].
2. Romero-Aroca P, Navarro-Gil R, Valls-Mateu A, Sagarra-Alamo R, Moreno-Ribas A, Soler N. Differences in incidence of diabetic retinopathy between type 1 and 2 diabetes mellitus: a nine-year follow-up study. Br J Ophthalmol 2017; 101:1346-51. [PMID: 28270484].
3. Kodjikian L, Bellocq D, Bandello F, Loewenstein A, Chakravarthy U, Koh A, Augustin A, de Smet MD, Chhablani J, Tufail A, García-Layana A, Sudhalkar A, Mathis T. First-line treatment algorithm and guidelines in center-involving diabetic macular edema. Eur J Ophthalmol 2019; 29:573-84. [PMID: 31238719].
4. Saeedi P, Petersohn I, Salpea P, Malanda B, Karuranga S, Unwin N, Colagiuri S, Guariguata L, Motala AA, Ogurtsova K, Shaw JE, Bright D, Williams R. IDF Diabetes Atlas Committee. Global and regional diabetes prevalence estimates for 2019 and projections for 2030 and 2045: Results from the International Diabetes Federation Diabetes Atlas, 9th edition. Diabetes Res Clin Pract 2019; 157:107843[PMID: 31518657].
5. Schmidt-Erfurth U, Garcia-Arumi J, Bandello F, Berg K, Chakravarthy U, Gerendas BS, Jonas J, Larsen M, Tadayoni R, Loewenstein A. Guidelines for the Management of Diabetic Macular Edema by the European Society of Retina Specialists (EURETINA). Ophthalmologica Journal international d'ophtalmologie International journal of ophthalmology Z Augenheilkd 2017; 237:185-222. .
6. Tan GS, Cheung N, Simó R, Cheung GC, Wong TY. Diabetic macular oedema. Lancet Diabetes Endocrinol 2017; 5:143-55. [PMID: 27496796].
7. Blindbaek SL, Peto T, Grauslund J. Aflibercept and navigated versus conventional laser in diabetic macular oedema: a 12-month randomized clinical trial. Acta Ophthalmol 2020; 98:347-52. [PMID: 31602811].
8. Kodjikian L, Bandello F, de Smet M, Dot C, Zarranz-Ventura J, Loewenstein A, Sudhalkar A, Bilgic A, Cunha-Vaz J, Dirven W, Behar-Cohen F, Mathis T. Fluocinolone acetonide implant in diabetic macular edema: International experts' panel consensus guidelines and treatment algorithm. Eur J Ophthalmol 2022; 32:1890-9. [PMID: 35139688].
9. Hansen MS, Rasmussen M, Grauslund J, Subhi Y, Cehofski LJ. Proteomic analysis of vitreous humour of eyes with diabetic macular oedema: a systematic review. Acta Ophthalmol 2022; 100:e1043-51. [PMID: 35507578].
10. Cehofski LJ, Honoré B, Vorum H. A Review: Proteomics in Retinal Artery Occlusion, Retinal Vein Occlusion, Diabetic Retinopathy and Acquired Macular Disorders. Int J Mol Sci 2017; 18:907-[PMID: 28452939].
11. Cehofski LJ, Kruse A, Mæng MO, Sejergaard BF, Schlosser A, Sorensen GL, Grauslund J, Honoré B, Vorum H. Dexamethasone Intravitreal Implant Is Active at the Molecular Level Eight Weeks after Implantation in Experimental Central Retinal Vein Occlusion. Molecules 2022; 27:5687-[PMID: 36080454].
12. Cehofski LJ, Kruse A, Alsing AN, Nielsen JE, Pedersen S, Kirkeby S, Honoré B, Vorum H. Intravitreal bevacizumab upregulates transthyretin in experimental branch retinal vein occlusion. Mol Vis 2018; 24:759-66. [PMID: 30581282].
13. Cehofski LJ, Kojima K, Terao N, Kitazawa K, Thineshkumar S, Grauslund J, Vorum H, Honoré B. Aqueous Fibronectin Correlates With Severity of Macular Edema and Visual Acuity in Patients With Branch Retinal Vein Occlusion: A Proteome Study. Invest Ophthalmol Vis Sci 2020; 61:6-[PMID: 33270842].
14. Cehofski LJ, Kojima K, Kusada N, Rasmussen M, Muttuvelu DV, Grauslund J, Vorum H, Honoré B. Macular Edema in Central Retinal Vein Occlusion Correlates With Aqueous Fibrinogen Alpha Chain. Invest Ophthalmol Vis Sci 2023; 64:23-[PMID: 36820679].
15. Honoré B. Proteomic Protocols for Differential Protein Expression Analyses. Methods Mol Biol 2020; 2110:47-58. [PMID: 32002900].
16. Tyanova S, Temu T, Cox J. The MaxQuant computational platform for mass spectrometry-based shotgun proteomics. Nat Protoc 2016; 11:2301-19. [PMID: 27809316].
17. Tyanova S, Temu T, Sinitcyn P, Carlson A, Hein MY, Geiger T, Mann M, Cox J. The Perseus computational platform for comprehensive analysis of (prote)omics data. Nat Methods 2016; 13:731-40. [PMID: 27348712].
18. Tusher VG, Tibshirani R, Chu G. Significance analysis of microarrays applied to the ionizing radiation response. Proc Natl Acad Sci U S A 2001; 98:5116-21. [PMID: 11309499].
19. Garcia-Moreno A, López-Domínguez R, Villatoro-García JA, Ramirez-Mena A, Aparicio-Puerta E, Hackenberg M, Pascual-Montano A, Carmona-Saez P. Functional Enrichment Analysis of Regulatory Elements. Biomedicines 2022; 10:590-[PMID: 35327392].

20. Cehofski LJ, Kruse A, Kjærgaard B, Stensballe A, Honoré B, Vorum H. Proteins involved in focal adhesion signaling pathways are differentially regulated in experimental branch retinal vein occlusion. Exp Eye Res 2015; 138:87-95. [PMID: 26086079].

21. Szklarczyk D, Franceschini A, Wyder S, Forslund K, Heller D, Huerta-Cepas J, Simonovic M, Roth A, Santos A, Tsafou KP, Kuhn M, Bork P, Jensen LJ, von Mering C. STRING v10: protein-protein interaction networks, integrated over the tree of life. Nucleic Acids Res 2015; 43:D447-52. [PMID: 25352553].

22. Szklarczyk D, Gable AL, Lyon D, Junge A, Wyder S, Huerta-Cepas J, Simonovic M, Doncheva NT, Morris JH, Bork P, Jensen LJ, Mering CV. STRING v11: protein-protein association networks with increased coverage, supporting functional discovery in genome-wide experimental datasets. Nucleic Acids Res 2019; 47:D1D607-13. [PMID: 30476243].

23. Szklarczyk D, Morris JH, Cook H, Kuhn M, Wyder S, Simonovic M, Santos A, Doncheva NT, Roth A, Bork P, Jensen LJ, von Mering C. The STRING database in 2017: quality-controlled protein-protein association networks, made broadly accessible. Nucleic Acids Res 2017; 45:D1D362-8. [PMID: 27924014].

24. Witmer AN, van den Born J, Vrensen GF, Schlingemann RO. Vascular localization of heparan sulfate proteoglycans in retinas of patients with diabetes mellitus and in VEGF-induced retinopathy using domain-specific antibodies. Curr Eye Res 2001; 22:190-7. [PMID: 11462155].

25. Schlingemann RO, Hofman P, Vrensen GF, Blaauwgeers HG. Increased expression of endothelial antigen PAL-E in human diabetic retinopathy correlates with microvascular leakage. Diabetologia 1999; 42:596-602. [PMID: 10333053].

26. Iglicki M, Busch C, Zur D, Okada M, Mariussi M, Chhablani JK, Cebeci Z, Fraser-Bell S, Chaikitmongkol V, Couturier A, Giancipoli E, Lupidi M, Rodríguez-Valdés PJ, Rehak M, Fung AT, Goldstein M, Loewenstein A. DEXAMETHASONE IMPLANT FOR DIABETIC MACULAR EDEMA IN NAIVE COMPARED WITH REFRACTORY EYES: The International Retina Group Real-Life 24-Month Multicenter Study. The IRGREL-DEX Study. Retina 2019; 39:44-51. [PMID: 29697589].

27. Chew EY. Patients With Good Vision and Diabetic Macular Edema Involving the Center of the Macula: To Treat or Not to Treat? JAMA 2019; 321:1873-5. [PMID: 31037295].

28. Bosma EK, van Noorden CJF, Schlingemann RO, Klaassen I. The role of plasmalemma vesicle-associated protein in pathological breakdown of blood-brain and blood-retinal barriers: potential novel therapeutic target for cerebral edema and diabetic macular edema. Fluids Barriers CNS 2018; 15:24-[PMID: 30231925].

29. Petersen MA, Ryu JK, Akassoglou K. Fibrinogen in neurological diseases: mechanisms, imaging and therapeutics. Nat Rev Neurosci 2018; 19:283-301. [PMID: 29618808].

30. Stasi A, Intini A, Divella C, Franzin R, Montemurno E, Grandaliano G, Ronco C, Fiaccadori E, Pertosa GB, Gesualdo L, Castellano G. Emerging role of Lipopolysaccharide binding protein in sepsis-induced acute kidney injury. Nephrol Dial Transplant 2017; 32:24-31. [PMID: 27387474].

31. Krasity BC, Troll JV, Lehnert EM, Hackett KT, Dillard JP, Apicella MA, Goldman WE, Weiss JP, McFall-Ngai MJ. Structural and functional features of a developmentally regulated lipopolysaccharide-binding protein. mBio 2015; 6:e01193-15. [PMID: 26463160].

32. Lehnert M, Uehara T, Bradford BU, Lind H, Zhong Z, Brenner DA, Marzi I, Lemasters JJ. Lipopolysaccharide-binding protein modulates hepatic damage and the inflammatory response after hemorrhagic shock and resuscitation. Am J Physiol Gastrointest Liver Physiol 2006; 291:G456-63. [PMID: 16614372].

33. Harman JC, Guidry JJ, Gidday JM. Intermittent Hypoxia Promotes Functional Neuroprotection from Retinal Ischemia in Untreated First-Generation Offspring: Proteomic Mechanistic Insights. Invest Ophthalmol Vis Sci 2020; 61:15-[PMID: 32910134].

34. Kunze A, Abari E, Semkova I, Paulsson M, Hartmann U. Deposition of nidogens and other basement membrane proteins in the young and aging mouse retina. Ophthalmic Res 2010; 43:108-12. [PMID: 19829017].

35. Gubbiotti MA, Neill T, Iozzo RV. A current view of perlecan in physiology and pathology: A mosaic of functions. Matrix biology: journal of the International Society for Matrix Biology 2017; 57:285–98.

36. Clements R, Turk R, Campbell KP, Wright KM. Dystroglycan Maintains Inner Limiting Membrane Integrity to Coordinate Retinal Development. J Neurosci 2017; 37:8559-74. [PMID: 28760865].

37. Montanaro F, Carbonetto S, Campbell KP, Lindenbaum M. Dystroglycan expression in the wild type and mdx mouse neural retina: synaptic colocalization with dystrophin, dystrophin-related protein but not laminin. J Neurosci Res 1995; 42:528-38. [PMID: 8568939].

38. Faralli JA, Filla MS, Peters DM. Role of Fibronectin in Primary Open Angle Glaucoma. Cells 2019; 8:1518-[PMID: 31779192].

39. Lemańska-Perek A, Adamik B. Fibronectin and its soluble EDA-FN isoform as biomarkers for inflammation and sepsis. Adv Clin Exp Med 2019; 28:1561-7. .

40. Miller CG, Budoff G, Prenner JL, Schwarzbauer JE. Minireview: Fibronectin in retinal disease. Exp Biol Med (Maywood) 2017; 242:1-7. [PMID: 27798121].

41. Bezerra JA, Carrick TL, Degen JL, Witte D, Degen SJ. Biological effects of targeted inactivation of hepatocyte growth factor-like protein in mice. J Clin Invest 1998; 101:1175-83. [PMID: 9486989].

42. Bezerra JA, Witte DP, Aronow BJ, Degen SJ. Hepatocyte-specific expression of the mouse hepatocyte growth factor-like protein. Hepatology 1993; 18:394-9. [PMID: 8340069].

43. Gurusamy D, Ruiz-Torres SJ, Johnson AL, Smith DA, Waltz SE. Hepatocyte growth factor-like protein is a positive

regulator of early mammary gland ductal morphogenesis. Mech Dev 2014; 133:11-22. [PMID: 25049204].

44. Ferone G, Mollo MR, Thomason HA, Antonini D, Zhou H, Ambrosio R, De Rosa L, Salvatore D, Getsios S, van Bokhoven H, Dixon J, Missero C. p63 control of desmosome gene expression and adhesion is compromised in AEC syndrome. Hum Mol Genet 2013; 22:531-43. [PMID: 23108156].

45. Ning M, Sarracino DA, Kho AT, Guo S, Lee SR, Krastins B, Buonanno FS, Vizcaíno JA, Orchard S, McMullin D, Wang X, Lo EH. Proteomic temporal profile of human brain endothelium after oxidative stress. Stroke 2011; 42:37-43. [PMID: 21164131].

46. Maes MB, Scharpé S, De Meester I. Dipeptidyl peptidase II (DPPII), a review. Clin Chim Acta 2007; 380:31-49. .

47. Danilova OV, Tai AK, Mele DA, Beinborn M, Leiter AB, Greenberg AS, Perfield JW 2nd, Defuria J, Singru PS, Lechan RM, Huber BT. Neurogenin 3-specific dipeptidyl peptidase-2 deficiency causes impaired glucose tolerance, insulin resistance, and visceral obesity. Endocrinology 2009; 150:5240-8. [PMID: 19819973].

48. Hernández C, García-Ramírez M, Colomé N, Corraliza L, García-Pascual L, Casado J, Canals F, Simó R. Identification of new pathogenic candidates for diabetic macular edema using fluorescence-based difference gel electrophoresis analysis. Diabetes Metab Res Rev 2013; 29:499-506. [PMID: 23568601].

49. Gao BB, Chen X, Timothy N, Aiello LP, Feener EP. Characterization of the vitreous proteome in diabetes without diabetic retinopathy and diabetes with proliferative diabetic retinopathy. J Proteome Res 2008; 7:2516-25. [PMID: 18433156].

50. Clermont A, Murugesan N, Zhou Q, Kita T, Robson PA, Rushbrooke LJ, Evans DM, Aiello LP, Feener EP. Plasma Kallikrein Mediates Vascular Endothelial Growth Factor-Induced Retinal Dysfunction and Thickening. Invest Ophthalmol Vis Sci 2016; 57:2390-9. [PMID: 27138737].

51. Sun JK, Maturi RK, Boyer DS, Wells JA, Gonzalez VH, Tansley R, Hernandez H, Maetzel A, Feener EP, Aiello LP. One-Time Intravitreal Injection of KVD001, a Plasma Kallikrein Inhibitor, in Patients with Central-Involved Diabetic Macular Edema and Reduced Vision: An Open-Label Phase 1B Study. Ophthalmol Retina 2019; 3:1107-9. [PMID: 31810575].

52. Kierans SJ, Taylor CT. Regulation of glycolysis by the hypoxia-inducible factor (HIF): implications for cellular physiology. J Physiol 2021; 599:23-37. [PMID: 33006160].

Articles are provided courtesy of Emory University and the Zhongshan Ophthalmic Center, Sun Yat-sen University, P.R. China. The print version of this article was created on 10 February 2024. This reflects all typographical corrections and errata to the article through that date. Details of any changes may be found in the online version of the article.